

from the pump laser was delivered by an optical fiber and was converted by second-harmonic-generation (SHG) to half its original wavelength by using an SHG crystal (β -BaB₂O₄). The resulting 775 nm SHG light was focused on the gap of a dipole-shaped low-temperature-grown GaAs (LTG-GaAs) PCA for THz generation (PCA1, length 7.5 μ m, width 10 μ m, gap 5 μ m). The pulsed THz radiation from PCA1 propagated in free space through two pairs of hemispherical silicon lenses (Si-L) and THz lenses (THz-L) and was then incident on another dipole-shaped LTG-GaAs PCA (PCA2) gated by the SHG light of the probe laser. A fully fiber-coupled THz spectrometer will be achieved without the need for frequency doubling if a PCA for a 1550 nm light is used [5]. Portions of the output light from the two lasers were fed into a sum-frequency-generation (SFG) cross correlator. The resulting SFG signal was used to generate a time origin signal in the AOS-THz-TDS mode. The current signal from PCA2 was amplified with a high-gain current preamplifier (AMP, bandwidth 100 kHz and sensitivity 5×10^7 V/A). The resulting voltage signal was measured with a fast digitizer by using the SFG signal as a trigger signal in the AOS-THz-TDS mode. In the case of the MFH-THz-CS mode, the signal was measured with a radio frequency (RF) spectrum analyzer, in place of the digitizer, without the need for the SFG cross correlator.

Figure 2(a) shows the temporal profile of the pulsed THz radiation measured in the AOS-THz-TDS mode, in which a single sweep measurement was carried out by the digitizer (required time 200 ms). A moderate dynamic range (DR) was achieved at the single sweep measurement. Figure 2(b) shows a power spectrum of the pulsed THz radiation obtained by a fast Fourier transform (FFT) of the temporal waveform in Fig. 2(a). A spectral range of 2 THz and DR of 100 was achieved at the acquisition time of 200 ms. Several absorption lines caused by atmospheric water vapor were clearly observed. For example, the absorption line at 0.556 THz has linewidth of 10 GHz, although the spectral resolution determined by the time window (350 ps) in Fig. 2(a) was 2.86 GHz. This linewidth is influenced by pressure broadening. Work is in progress to evaluate the actual spectral resolution by the THz spectroscopy of the low-pressure water vapor. The use of a broadband THz emitter, e.g., a DAST crystal [6], will permit further expansion of the spectral bandwidth, together with reducing the timing jitter of the dual fiber combs.

We next demonstrated the MFH-THz-CS mode using the same spectrometer. In this mode, an electromagnetic THz comb (EM-THz comb, frequency spacing f_1) is radiated from PCA1 excited by the SHG optical comb of the pump light, whereas a photocarrier THz comb (PC-THz comb, frequency spacing $f_2 = f_1 + \Delta f$) is induced in PCA2 gated by that of the probe light [3]. When the free-space-propagating EM-THz comb is incident on PCA2 having the PC-THz comb, a secondary frequency comb having the frequency spacing of Δf is observed in the RF region via the multifrequency-heterodyning photoconductive process occurring between the EM-THz and PC-THz combs. Since the observed RF comb is a replica of the EM-THz comb scaled down by $f_1/\Delta f = 11,224,800$ in frequency, one can reconstruct the EM-THz comb easily via direct observation of the

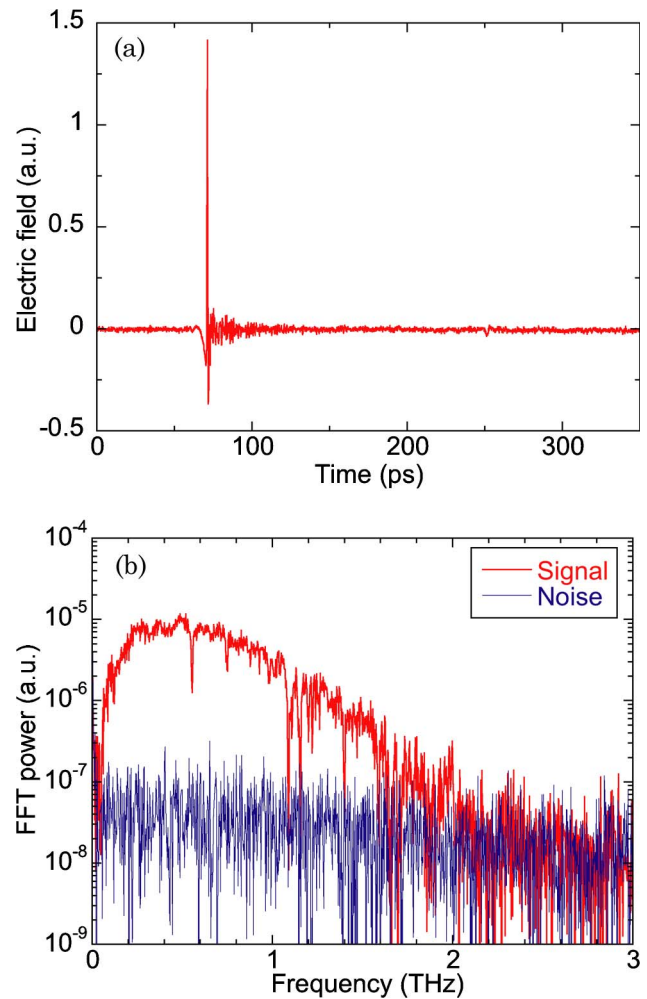


Fig. 2. (Color online) (a) Temporal waveform and (b) power spectrum of the pulsed THz radiation measured at the single sweep measurement in AOS-THz-TDS mode (acquisition time 200 ms).

RF comb by using the RF spectrum analyzer and by calibration of the frequency scale using $f_1/\Delta f$, without the need for FFT calculation. Figure 3(a) shows a power spectrum of the EM-THz comb measured in the MFH-THz-CS mode (measurement time 100 s). The spectrum of the EM-THz comb, here plotted in red, is actually composed of a series of frequency spikes regularly separated by the mode-locked frequency. Also, the absorption lines caused by the water vapor were confirmed. For comparison, the THz power spectrum was measured at the same measurement time in AOS-THz-TDS mode as shown in Fig. 3(b), in which signal averaging of 500-sweep sequences was carried out by the digitizer. Although the actual -10 dB bandwidth of the MFH-THz-CS mode (1.286 THz) was almost equal to that of the AOS-THz-TDS mode (1.230 THz), there was a large difference in DR between the two modes; this leads to difference of the spectral tail between them. The spectral bandwidth and DR in the MFH-THz-CS mode should be equal to those in the AOS-THz-TDS mode because both of these modes share the same dual fiber combs and PCAs. The only difference between the two modes is the measuring instrument: the digitizer for the AOS-THz-TDS mode and the spectrum analyzer for the MFH-THz-CS mode. The

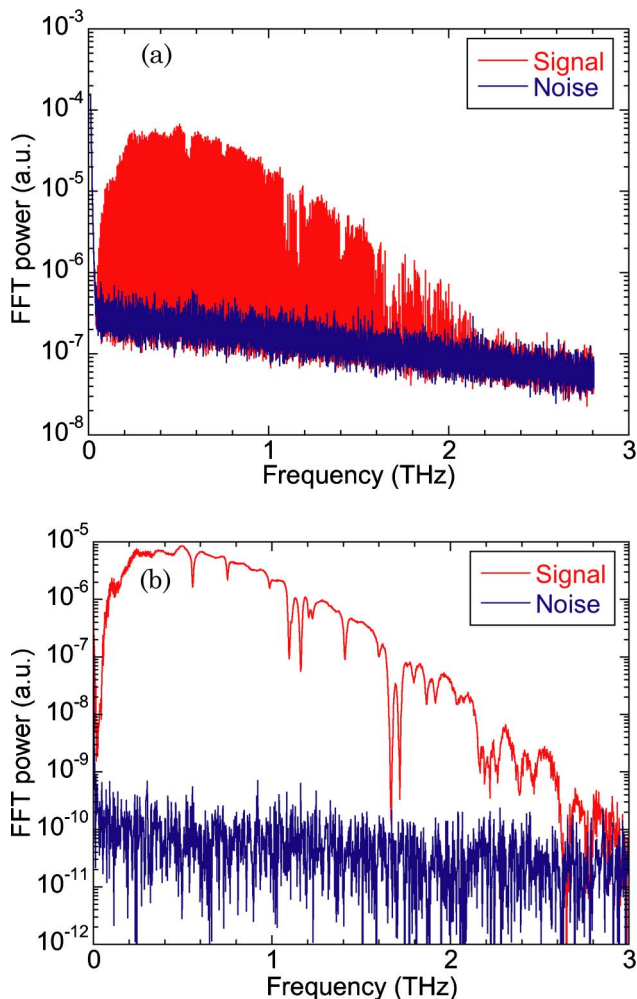


Fig. 3. (Color online) Comparison of power spectrum measured in (a) MFH-THz-CS mode (sweep time 100 s) and (b) AOS-THz-TDS mode (acquisition time 100 s).

digitizer can capture the signal components of the pulsed THz radiation in the time domain. Conversely, since our spectrum analyzer is based on the superheterodyne technique, it acquires only the frequency-component signal coinciding with the frequency of its local oscillator at any given moment, and then acquires the overall spectrum by sweeping the frequency of the local oscillator. Although this superheterodyne technique can enhance

a weak signal by heterodyning with the signal of the local oscillator, it is likely that the efficiency of signal acquisition in the spectrum analyzer is still lower than that in the digitizer in this demonstration. However, if the zero-span mode is used in the spectrum analyzer, the MFH-THz-CS mode has the advantage of real-time monitoring capability of the THz amplitude at a single frequency, such as a specified THz spectral fingerprint.

In conclusion, we have constructed a fiber-based, hybrid THz spectrometer, working in the AOS-THz-TDS mode and the MFH-THz-CS mode, by use of dual fiber combs. We compared the basic performance between both modes and found that the former mode is superior to the latter mode in terms of DR, although the latter mode offers real-time monitoring capability of the THz amplitude at an arbitrary, single frequency, in addition to a simple setup without the need for FFT calculation and an SFG cross-correlator. The constructed spectrometer is expected to become a compact, alignment-free, robust, flexible, and cost-effective apparatus suitable for practical applications.

This work was supported by Grants-in-Aid for Scientific Research 20560036, 21360039, and 21650111 from the Ministry of Education, Culture, Sports, Science, and Technology of Japan. We also gratefully acknowledge financial support from the Renovation Center of Instruments for Science Education and Technology in Osaka University, the Suzuki Foundation and the Mitutoyo Association for Science and Technology, Japan.

References

1. T. Yasui, E. Saneyoshi, and T. Araki, *Appl. Phys. Lett.* **87**, 061101 (2005).
2. A. Bartels, A. Thoma, C. Janke, T. Dekorsy, A. Dreyhaupt, S. Winnerl, and M. Helm, *Opt. Express* **14**, 430–437 (2006).
3. T. Yasui, Y. Kabetani, E. Saneyoshi, S. Yokoyama, and T. Araki, *Appl. Phys. Lett.* **88**, 241104 (2006).
4. H. Inaba, Y. Daimon, F.-L. Hong, A. Onae, K. Minoshima, T. R. Schibli, H. Matsumoto, M. Hirano, T. Okuno, M. Onishi, and M. Nakazawa, *Opt. Express* **14**, 5223 (2006).
5. B. Sartorius, H. Roehle, H. Künzel, J. Böttcher, M. Schlak, D. Stanze, H. Venghaus, and M. Schell, *Opt. Express* **16**, 9565 (2008).
6. J. Takayanagi, S. Kanamori, K. Suizu, M. Yamashita, T. Ouchi, S. Kasai, H. Ohtake, H. Uchida, N. Nishizawa, and K. Kawase, *Opt. Express* **16**, 12859 (2008).